# Lithium Ion Intercalation Performance of Porous Laminal Titanium Dioxides Synthesized by Sol−Gel Process

Min-Chiao Tsai,[†] Jian-Chia Chang,[†] Hwo-Shuenn Sheu,[‡] Hsin-Tien Chiu,[§] and Chi-Young Lee[†,⊥,*]

*Department of Materials Science and Engineering, Center for Nanotechnology, Materials Science and Microsystems, National Tsing Hua University, Hsinchu, Taiwan, Synchrotron Radiation Research Center, Hsinchu, Taiwan, and Department of Applied Chemistry, National Chiao Tung University, Hsinchu, Taiwan*

*Received August 29, 2008. Revised Manuscript Received November 22, 2008*

We have synthesized novel mesoporous titanate nanosheets by reacting titanium isopropoxide (TTIP) with formic acid. The porous nanosheets were characterized as a new titanate structure with intercalation of formate groups and protons, in the form of HCOOH-intercalated titanate. Most interestingly, $TiO_2$−B, a well-known but unusual titanium dioxide phase with great potential in applications in Li-ion batteries, was obtained after the nanosheets were heated above 250 °C. Mesoporous nanosheets of HCOOH-intercalated titanate, titanium dioxide with mostly $TiO_2$−B and titanium dioxide with traces of $TiO_2$−B were obtained by heating the as prepared mesoporous titanate nanosheets at 200, 300, and 550 °C, respectively. The method reported here is the first to utilize the sol−gel process to synthesize $TiO_2$−B. In addition, different anodes were made from HCOOH-intercalated titanate and titanium dioxide with different ratios of $TiO_2$−B to examine the performance of the charging/discharging capacity in Li ion intercalation. The discharging capacity of titanium dioxide with major $TiO_2$−B can reach 357 mA h/g at the first charging cycle and is highest among $TiO_2$−B reports so far.

## Introduction

In the past few decades, titanium-related materials such as titanate,[1] titanium carboxylate,[2] and especially $TiO_2$ have attracted a lot of attention because of their abundant applications in scattering color filters,[3] photocatalysts,[4] solar cells,[5] and hydrogen storage.[6] In recent years, scientists have shifted their focus to using $TiO_2$ as the anode in Li ion batteries. There are several advantages for replacing graphite with $TiO_2$ as the anodic materials, including lower cost and higher charging/discharging rate. Particularly, safety is improved as the formation of Li metal dendrites is prevented that would pierce the separator in a cell. The Li ion intercalation voltage and discharging/charging window (1−3 V versus Li+/Li) of a $TiO_2$ anode are much further from the Li+/Li redox couple than that of a graphite anode. This prevents the formation of Li metal dendrites, which could pierce the separator membrane of a cell. The capacity performance of anodes made by the most of polymorphs of $TiO_2$ such as anatase,[7] rutile,[8] $TiO_2$−H (hollandite),[9] $TiO_2$−R (ramsdellite),[10] even amorphous titanium oxide[11] has been demonstrated. The maximum insertion amount of Li could reach nearly 0.8 of unit $TiO_2$ ($Li_{0.8}TiO_2$) resulting in 268 mA h/g at 1−3 V versus $Li^+$/Li and retained with long life and high charging/discharging rate on cycling.[7,10,11]

Among different titanium oxide materials, the unusual phase $TiO_2$−B has gradually become more prominent in energy storage because of its relatively open structure. $TiO_2$ phases are all constructed of titanium-centered $TiO_6$ octahedrons with edge-sharing or corner oxygen atoms. Unlike the conventional anatase and rutile, the less dense $TiO_2$−B phase has channels along the *c* axis and voids in the (001) plane making it a good candidate as an intercalation host. Armstrong and co-workers prepared $TiO_2$−B nanotube and nanowire anodes that could accommodate Li ion insertion

* Corresponding author. E-mail: cylee@mx.nthu.edu.tw. Tel: 886 3 5715131-42570.
† Department of Materials Science and Engineering, National Tsing Hua University.
‡ Synchrotron Radiation Research Center.
§ National Chiao Tung University.
⊥ Center for Nanotechnology, Materials Science and Microsystems, National Tsing Hua University.

(1) Bavykin, D. V.; Friedrich, J. M.; Walsh, F. C. *Adv. Mater.* **2006**, *18*, 2807.
(2) Chen, Q.; Zhou, W. Z.; Du, G. H.; Peng, L. M. *Adv. Mater.* **2002**, *14*, 1208.
(3) Tsai, M. C.; Tsai, T. L.; Lin, C. T.; Chung, R. J.; Sheu, H. S.; Chiu, H. T.; Lee, C. Y. *J. Phys. Chem. C* **2008**, *112*, 2697.
(4) Martinez-Ferrero, E.; Sakatani, Y.; Boissiere, C.; Grosso, D.; Fuertes, A.; Fraxedas, J.; Sanchez, C. *Adv. Funct. Mater.* **2007**, *17*, 3348.
(5) (a) Iskandar, F.; Nandiyanto, A. B. D.; Yun, K. M.; Hogan, C. J.; Okuyama, K.; Biswas, P. *Adv. Mater.* **2007**, *19*, 1408. (b) Kang, S. H.; Choi, S. H.; Kang, M. S.; Kim, J. Y.; Kim, H. S.; Hyeon, T.; Sung, Y. E. *Adv. Mater.* **2008**, *20*, 54. (c) Zhang, D. S.; Yoshida, T.; Oekermann, T.; Furuta, K.; Minoura, H. *Adv. Funct. Mater.* **2006**, *16*, 1228.
(6) Mor, G. K.; Shankar, K.; Paulose, M.; Varghese, O. K.; Grimes, C. A. *Nano Lett.* **2006**, *6*, 215.
(7) Sudant, G.; Baudrin, E.; Larcher, D.; Tarascon, J. M. *J. Mater. Chem.* **2005**, *15*, 1263.
(8) Hu, Y. S.; Kienle, L.; Guo, Y. G.; Maier, J. *Adv. Mater.* **2006**, *18*, 1421.
(9) Noailles, L. D.; Johnson, C. S.; Vaughey, J. T.; Thackeray, M. M. *J. Power Sources* **1999**, *82*, 259.
(10) Kuhn, A.; Amandi, R.; Garcia-Alvarado, F. *J. Power Sources* **2001**, *92*, 221.
(11) Hibino, M.; Abe, K.; Mochizuki, M.; Miyayama, M. *J. Power Sources* **2004**, *126*, 139.

10.1021/cm802327z CCC: $40.75 
Published on Web 01/05/2009

as high as $Li_{0.9}TiO_2$ (305 mA h/g) during the first cycle,[12,13] which is generally much better than other $TiO_2$ polymorphs. Although $TiO_2$−B anodes were excellent in the capacity performance of Li ion batteries, the scientific evolution of $TiO_2$−B was more sluggish than the other two popular $TiO_2$ phases, anatase and rutile. The most important reason is that reported syntheses of $TiO_2$−B are quite rare, especially that of nanostructures. Generally, the process involves heat treatment of titanate samples obtained from ion-exchanged sodium titanate which is synthesized form reacting titanium dioxide powder with a concentrated NaOH solution at 100 °C for two days. The temperature of heating is quite critical and usually ranges from 250 to 500 °C for the transformation of hydrogen titanate to $TiO_2$−B. Because $TiO_2$−B is metastable, it can easily convert to the anatase phase at higher temperatures. Herein, we report a novel sol−gel method to prepare sheetlike titanate and $TiO_2$−B. In particular, the nanosheets are mesoporous instead of having a solid inner structure. It has been demonstrated that nanostructue anodes perform better in capacity and life cycles than anodes made from bulk materials[7] because nanosized materials provide higher contact area between electrode and electrolyte, shorter diffusion lengths for both Li ion and electron transport and increased durability against the strain of Li ion intercalation and extraction. The fact that this is a two-step process is also of merit compared to the typical synthesis, which can be far more complex.

## Experimental Section

All chemicals in this work were purchased from the Aldrich Company and used directly without any pretreatment. 0.03 mL (1 mmol) titanium isopropoxide (TTIP, 97%, Aldrich) were reacted with 20 mL formic acid (98−100%) at 150 °C under reflux. The reaction proceeded rapidly and was accompanied by the instantaneous appearance of a pale yellow precipitate. The mixture was stirred for several minutes to ensure that the reaction has gone to completion then the flask was placed in 150 °C silicon oil bath. Different reaction times were allowed in order to follow the entire formation procedure (0, 1, 2, and 6 days). After the reaction, the product was washed several times with formic acid and under a vacuum for 1 h to remove solvent. The products were heated under air from 150 to 550 °C through a temperature heating rate of 5 °C per min over 4 h and then cooled to room temperature.

Electrochemical cells consisted of a $TiO_2$/carbon composite as the negative electrode, lithium metal as the counter electrode, and an electrolyte of 1 M LiPF6 in ethylene carbonate (EC)/ethyl methyl carbonate (EMC)/propylene carbonate (PC)/dimethyl carbonate (DMC) (3:4:1:2 vol %). A Celgard 2400 membrane was used as the cell separator. The anode was mixture of 80 wt % $TiO_2$, 10 wt % carbon black, and 10 wt % polyvinylidene fluoride (PVDF) as binder. The cells were assembled in an argon-filled glovebox and charge/discharge cycle tests were performed using an Arbin BT2000 at a constant current density, with cutoff voltage of 3.0 to 1.0 V.

SEM images were taken with a JEOL-6500 scanning electron microscope. TEM images were obtained with a JEOL-2010 transmission electron microscope with an accelerating voltage of 200 kV and X-ray diffraction patterns were all acquired at the National Synchrotron Radiation Research Center (01C beam line). The incident X-ray energy in this work was 13 keV (wavelength = 0.9537Å).

## Results and Discussions

Synthesis of nanosheets via a typical sol−gel process usually involves two steps, hydrolysis and condensation of metal alkoxides. In this work, we used titanium isopropoxide (TTIP) and formic acid as both precursor and solvent. The reaction occurred rapidly, with the immediate precipitating of a white powder when TTIP was injected into the formic acid solution. It is known that different carboxylic acids such as acetic acid and valeric acid can retard hydrolysis rates to different extents to avoid premature precipitation in the sol−gel process.[3] However, excess carboxylic acid has an opposite effect and accelerates the formation of precipitate due to local esterification around TTIP.[14] This in turn produces large amount of water, which triggers a series of hydrolysis and condensation.

Figure 1A shows the SEM image of the precipitate at the initial stage of the reaction. It is an aggregation of irregular particles ranging form 50 to 200 nm which resembles typical products of a sol−gel process. Gradually, the nanoparticles anisotropically transformed to one-dimensional structures after 24 h (Figure 1B). As the reaction progressed, planar products appeared and became the major component of the powders after 48 h (images C and D in Figure 1). In some regions, traces of the initial one-dimensional structures were still observed (see the Supporting Information, Figure S1a). Belt- or sheetlike products appeared to form by lateral connection of nanowires formed prior, whereas sodium titanate and hydrogen titanate nanowires, prepared from hydrothermal treatment of $TiO_2$ powder in NaOH solution, remain independent nanowires. The nanosheets are of different sizes but of uniform thickness, about 30−50 nm.

The microstructure transformation was monitored through the X-ray diffraction patterns (XRD) shown in Figure 2. The initial precipitates with particle shape were amorphous and no obvious peaks were observed in the XRD pattern (black line). The belt-like products obtained after 24 h of reaction showed some broad peaks with large fwhm which denotes the formation of short-range order structures appearing at $2\theta$ = 15.6, 23.2, 29.0, 32.6, and 33.1°. The peaks can be assigned to the anatase phase of $TiO_2$ according to JCPDS data. As the reaction progresses, two more peaks appeared in the low $2\theta$ region, 7.76 and 9.2° matching the *d*-spacing 7.05 and 5.95 Å, respectively. Most significantly, peaks at $2\theta$ values equal to 15.6 and 29.0, related to the lattice spacing of 3.51 and 1.90 Å, respectively. Because anatase, $TiO_2$−B, and most titanates are constructed of zigzag sheets of $TiO_6$ octahedrons, the spacings are usually about 3.6 and 1.9 Å, which is consistent with what was observed with this material.

To obtain more information of microstructure, the lamina material was studied by ED and HRTEM (Figure 3). A HRTEM study in Figure 3A shows distinct fringes with large spacings, the *d*-spacings of the two sets of planes are 7.1

(12) (a) Armstrong, A. R.; Armstrong, G.; Canales, J.; Bruce, P. G. *Angew. Chem., Int. Ed.* **2004**, *43*, 2286. (b) Armstrong, A. R.; Armstrong, G.; Canales, J.; Garcia, R.; Bruce, P. G. *Adv. Mater.* **2005**, *17*, 862.

(13) Armstrong, G.; Armstrong, A. R.; Canales, J.; Bruce, P. G. *Chem. Commun.* **2005**, 2454.

(14) Sanchez, C.; Livage, J. *New J. Chem.* **1990**, *14*, 513.

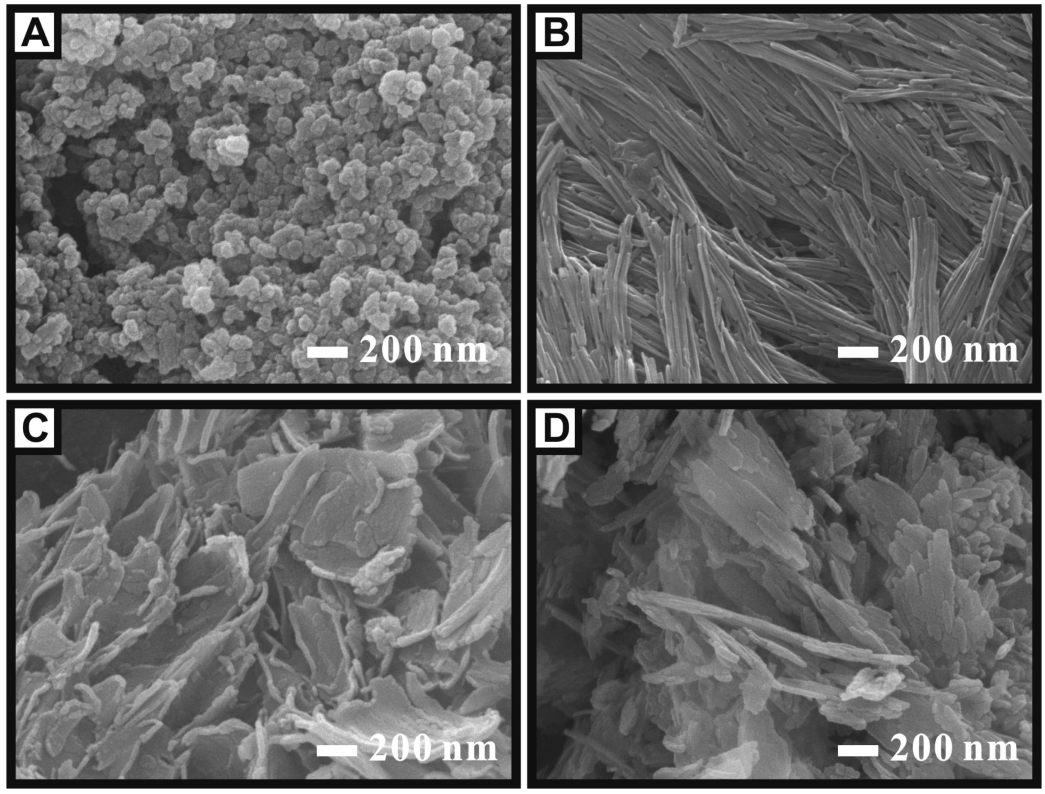


**Figure 1.** SEM images of HCOOH-intercalated titanates after different reaction times: (A) 0, (B) 24, (C) 48, and (D) 144 h.

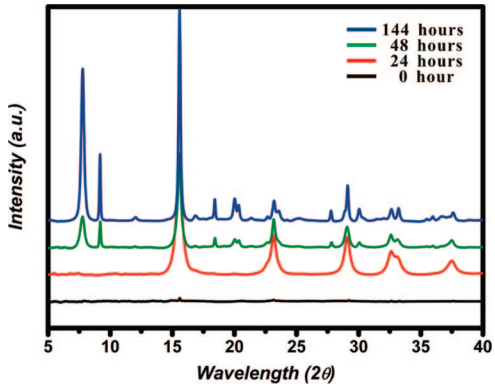


**Figure 2.** X-ray diffraction patterns (XRD) of HCOOH-intercalated titanates after different reaction times: (A) 0, (B) 24, (C) 48, and (D) 144 h.

and 6.0 Å with a dihedral angle of 44.0°, estimated by the FFT in the inset. As we know, there are two sets of planes with large spacings assigned to (001) and (200) in $TiO_2$−B, but the dihedral angle between the planes is much larger than 44.0°. Furthermore, large plane spacings assigned to (200) and (20$\bar{1}$) are usually observed in various titanates, for example $H_2Ti_3O_7$, $H_2Ti_4O_9 \cdot H_20$, $K_2Ti_6O_{13}$.[15] On the basis of these similarities, we predict that the structure of these nanosheets is very close to titanate and $TiO_2$−B, composed of the "stepped sheets" through edge-sharing oxygen atoms. However, a well-fitted XRD pattern of conventional titanates was not found for this structure. These observations strongly suggest that the lamina material is a new titanate.

A closer examination of the lamina material revealed that the nanosheets are not solid but with numerous 5−20 nm sized mesopores (images B and C in Figure 3). HRTEM image shows a void enclosed by a wall with distinct fringes with 3.51 Å lattice spacing. It should be noted that the nanosheets are very unstable under electron irradiation when TEM images are taken. The nanosheets were single crystalline in the initial seconds of electron irradiation as shown by the electron diffraction pattern (ED) in the inset of Figure 3B. However, the single-crystalline structure transformed very quickly to a polycrystalline structure with a ring pattern as seen in the ED after a few seconds (inset of Figure 3D) under the irradiation of electron beam of TEM.

New titanate is similar to hydrogen titanate in that it is also thermally unstable. TGA analysis of HCOOH-intercalated titanate shown in Figure 4A was carried out to examine thermal stability in detail. A weight loss of 2.3% contributed from desorption of water is observed below 200 °C. When heated over 200 °C, the weight loss gradually increases, reaching 30% under air or 35% under He gas at around 300 °C. The TGA analysis of new titanate is very different to sodium and hydrogen titanates in weight loss. The weight loss of HCOOH-intercalated titanate is much more than that of the other two titanates, which is usually in the range of 5−15%.[16]

The in situ mass (Figure 4B) and IR spectra (Figure 5) gave a clearer insight into this new structure. In Figure 4B, only two obvious peaks appear at $m/z = 18$ and 28, assigned to $H_2O^+$ and $CO^+$ fragments respectively, with an intensity ratio of 1/4 when the temperature reached 300 °C. It has

(15) (a) Nakahira, A.; Kato, W.; Tamai, M.; Isshiki, T.; Nishio, K.; Aritani, H. *J. Mater. Sci.* **2004**, *39*, 4239. (b) Du, G. H.; Chen, Q.; Han, P. D.; Yu, Y.; Peng, L. M. *Phys. Rev. B* **2003**, 67.

(16) (a) Morgado, E.; de Abreu, M. A. S.; Moure, G. T.; Marinkovic, B. A.; Jardim, P. M.; Araujo, A. S. *Chem. Mater.* **2007**, *19*, 665. (b) Sauvet, A. L.; Baliteau, S.; Lopez, C.; Fabry, P. *J. Solid State Chem.* **2004**, *177*, 4508.

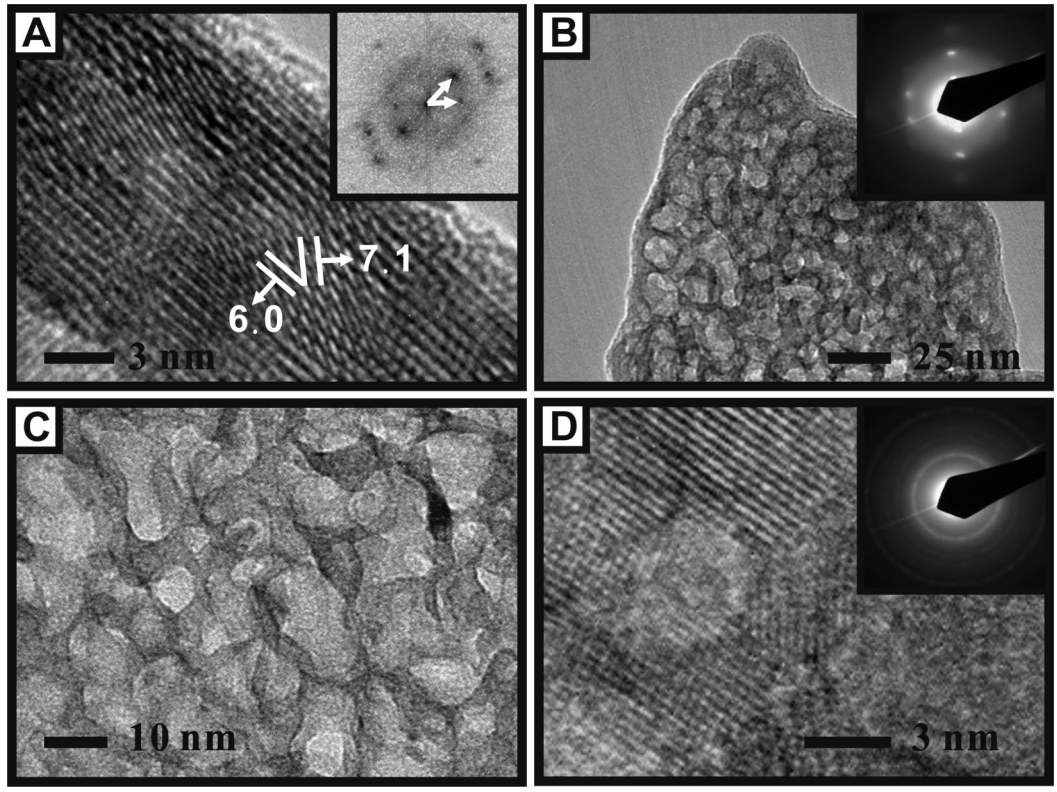


**Figure 3.** (A) HRTEM image of a nanosheet showing two sets of planes with large lattice spacing, 6.0 and 7.1 Å. The inset is the fast Fourier transformation of the HRTEM image. (B, C) TEM images of a nanosheet with different magnifications showing that there are numerous mesopores ranging from 5 to 20 nm. The inset is an electron diffraction pattern of the nanosheet at the beginning of electron irradiation. (D) Cear void of about 5 nm diameter surrounded by walls presented with lattice images. The inset is an electron diffraction pattern of the nanosheet after a few seconds of electron irradiation.

been established by experiments and simulations that formic acid dissociatively adsorbs more readily on the surface of anatase $TiO_2$ under most conditions.[17,18] The formate group can bind to the free coordination site on an unsaturated surface Ti atom ($Ti_{5c}$). The modes of binding can be monodentate, bidentate chelating, or bidentate bridging depending on the crystal plane and surface hydration, whereas the hydrogen atom of formic acid binds to a neighboring oxygen atom ($O_{2c}$), bridging two Ti atoms to form a hydroxyl group. On the other hand, molecular physisorption is only feasible at perfectly clean anatase (101) and fully hydrated (001) surfaces.[17,18] Therefore, we believe the formic acid is intercalated into the titanate layer structure in the form of a formate and a proton. The absence of a peak at $m/z = 46$, corresponding to complete formic acid, is evidence for this. In Figure 5, black and red lines denote IR spectra of the nanosheets heated at 200 and 300 °C, respectively. There are two groups of peaks located in the region between 1300 and 1600 $cm^{-1}$ which has been enlarged in the inset and can be roughly resolved into five peaks, 1353, 1371, 1388, 1524, and 1546 $cm^{-1}$. The peaks at 1353, 1388, and 1546 $cm^{-1}$ can be assigned to $\upsilon_s$(COOH), $\delta$(HCO) and $\upsilon_{as}$(COOH), respectively.[19] Furthermore, the frequency of the asymmetric stretch ($\upsilon_{as}$(COOH)) is more sensitive to the bonding surface, geometry and environment than that of the symmetric stretch ($\upsilon_s$(COOH)).[20,21] The frequency of asymmetric stretches usually range from 1530 to 1590 $cm^{-1}$, such as 1534 $cm^{-1}$ for adsorption of gaseous formic acid, 1548 $cm^{-1}$ for adsorption in solution, 1560 $cm^{-1}$ for adsorption on an oxygen defect, and 1580 $cm^{-1}$ for aqueous formate.[19−21] This is the first observation of such low frequency (1524 $cm^{-1}$) carbonate asymmetric stretches ($\upsilon_{as}$(COOH)). Thus, the peak at 1524 $cm^{-1}$ was probably assigned to the asymmetric stretch of formate in between the layers of titanate. On the basis of the above discussion, it has been concluded that formic acid will irreversibly dissociatively intercalate into the layer structure in a bidentate fashion. Considering this and TGA data, a possible formula for this material was derived as $TiO_2 \cdot (HCOOH)_{0.9}$, according to 35% weight loss under He carrier gas. Surprisingly, the ratio of HCOOH to $TiO_2$ is much higher than that of usual titanates, as the oxygen atoms of formate contribute to the octahedral $TiO_6$ framework. Thus, it was designated HCOOH-intercalated titanate. Although we propose that formates possibly participate in the construction of the HCOOH-intercalated titanate framwork, the detailed structure is still unknown, and work for this is still being carried out.

It is known that hydrogen titanate is metastable and very easily converted to $TiO_2$−B or anatase. Hence, we have

(17) (a) Gong, X. Q.; Selloni, A. *J. Catal.* **2007**, *249*, 134. (b) Tanner, R. E.; Sasahara, A.; Liang, Y.; Altman, E. I.; Hiroshi, O. *J. Phys. Chem. B* **2002**, *106*, 8211. (c) Gong, X. Q.; Selloni, A.; Vittadini, A. *J. Phys. Chem. B* **2006**, *110*, 2804.

(18) Vittadini, A.; Selloni, A.; Rotzinger, F. P.; Gratzel, M. *J. Phys. Chem. B* **2000**, *104*, 1300.

(19) Rotzinger, F. P.; Kesselman-Truttmann, J. M.; Hug, S. J.; Shklover, V.; Gratzel, M. *J. Phys. Chem. B* **2004**, *108*, 5004.

(20) Hayden, B. E.; King, A.; Newton, M. A. *J. Phys. Chem. B* **1999**, *103*, 203.

(21) Andersson, M.; Kiselev, A.; Osterlund, L.; Palmqvist, A. E. C. *J. Phys. Chem. C* **2007**, *111*, 6789.

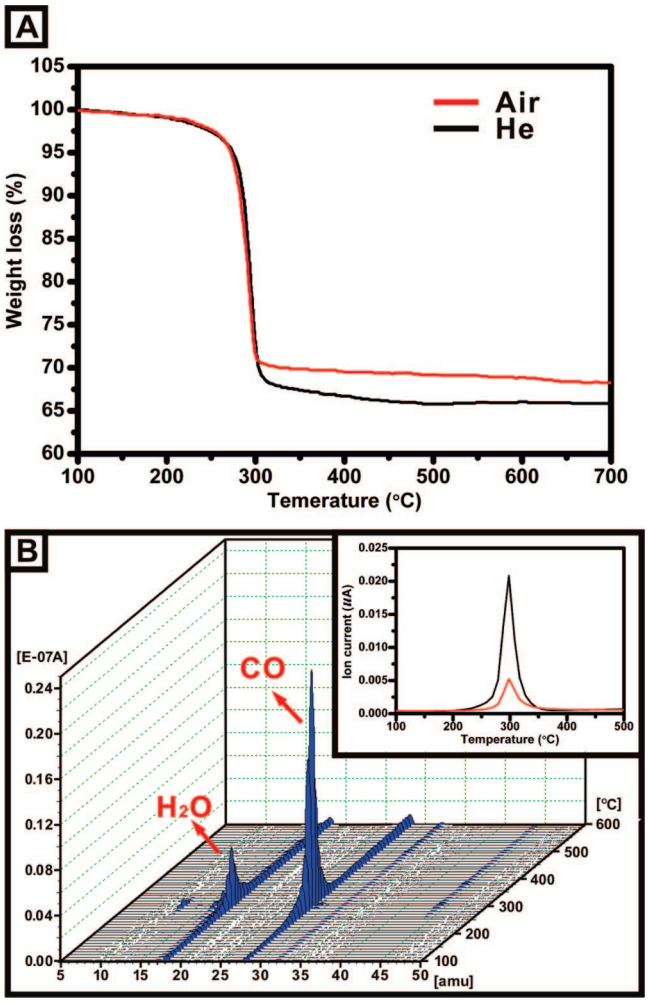


**Figure 4.** (A) TGA analysis of HCOOH-intercalated titanate under different gases. (B) In situ mass spectra present that peaks only appeared in the region less than 50 *m*/*z* in which the two most intense peaks, 18.25 and 28.25 *m*/*z*, are assigned to $H_2O$ and CO. The inset shows the trace of formation of CO and $H_2O$ molecules, black and red curves, with increasing temperature.

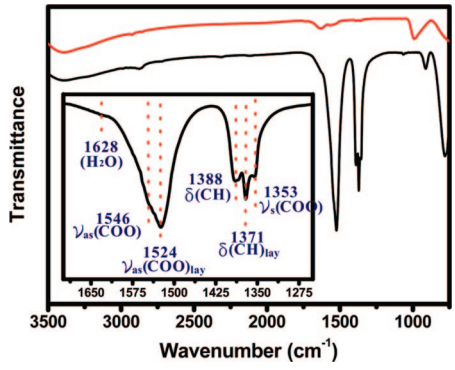


**Figure 5.** Infrared (IR) spectra of HCOOH-intercalated titanates after different heating temperatures. Black and red lines represent the IR spectra of HCOOH-intercalated titanates heated at 200 and 300 °C, respectively. The region between 1250 and 1700 $cm^{-1}$ is enlarged in the inset.

studied the transformation of HCOOH-intercalated titanate at various temperatures with the XRD patterns shown in Figure 6. The HCOOH-intercalated titanate structure persists below 200 °C; over 200 °C, it becomes unstable and changes into the $TiO_2$−B and anatase phases. The results are consistent with TGA and IR analysis in which most of the IR peaks assigned to formate adsorption disappeared as the

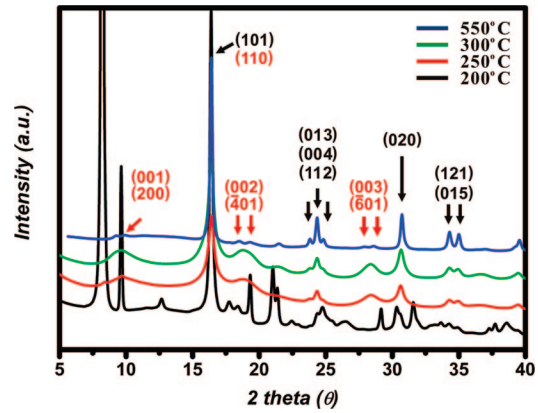


**Figure 6.** X-ray diffraction patterns (XRD) of HCOOH-intercalated titanates after different heating temperatures. Black and red arrows denote anatase and $TiO_2$−B phases, respectively, and crystalline planes also indexed with different colors.

**Table 1. Mole Percentage of Anatase and $TiO_2$−B Phases Calculated by Rietveld Refinement**

| *T* (°C) | anatase (%) | $TiO_2$−B (%) | $R_p$[a] | $R_{wp}$[b] |
|---|---|---|---|---|
| 300 | 49.7 ± 0.69 | 50.3 ± 1.26 | 0.0825 | 0.1127 |
| 550 | 94.7 ± 1.09 | 5.3 ± 0.56 | 0.0577 | 0.0752 |

[a] $R_p$ = reliability factor of profile. [b] $R_{wp}$ = weighted reliability factor.

powder was heated at 300 °C, only a peak at 1628 $cm^{-1}$ assigned to water adsorption remained. On the basis of the XRD pattern, $TiO_2$−B and anatase (Figure 6) are the dominant phases of the powder heated over 250 °C. HCOOH-intercalated titanate completely disappeared when heated above a temperature of 300 °C. To study detailed phase compositions, XRD patterns of samples at 300 and 550 °C were refined by Rietvled method with GSAS program to obtain the exact phase ratio and the results are presented in Table 1. The ratios of anatase and $TiO_2$−B at 300 and 500 °C are about 1:1 and 19:1, respectively. The grain size of anatase is much larger than that of $TiO_2$−B at 300 °C according to its diffraction peak width. However, the size effect, which broadens the width and decreases the diffraction intensity, does not specially take into account in the Rietveld refinement so that the quantity of $TiO_2$−B would be undervalued in the sample at 300 °C. Moreover, it is worth noting that a certain amount of $TiO_2$−B, 5.3%, still exists at 550 °C in spite of the weak intensity of $TiO_2$−B peaks. These peaks are usually buried in the background noise when a commercial XRD instrument is used. Thus, a more powerful X-ray source like synchrotron radiation could be used to examine the existence of $TiO_2$−B although $TiO_2$−B seemed not to contribute to Li-ion battery capacity at such low quantities. Also, the reaction should be carefully tuned in order to obtain the highest ratio of $TiO_2$−B.

Furthermore, the capability for Li-ion intercalation of different $TiO_2$ was examined by making Li-ion battery anodes with different $TiO_2$. According to the results of XRD refinements, HCOOH-intercalated titanate, $TiO_2$−B and anatase are the dominant phases of the powder heated at 200, 300, and 550 °C, respectively. Figure 7 shows the capacity charging/discharging results of three anodes made from different $TiO_2$ at 1−3 V versus $Li^+$/Li. Among these, the discharging capacity of the HCOOH-intercalated titanate anode is largest at up to 440 mA h/g, which is much higher

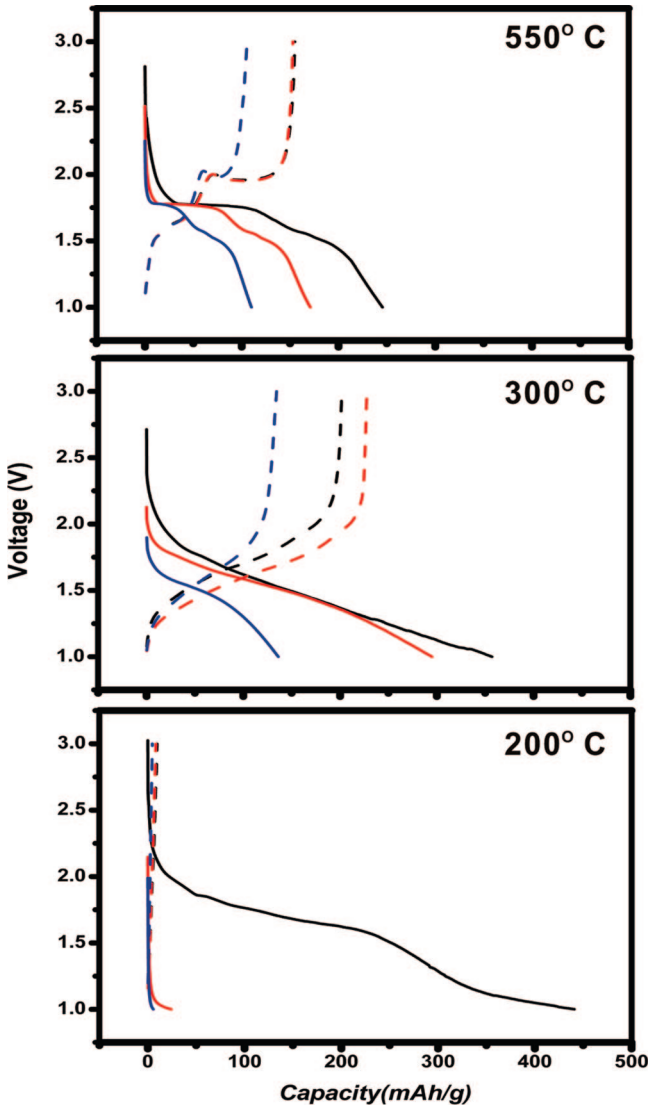


**Figure 7.** Charging/discharging curves of three different anodes at potential 3−1 V versus $Li^+$/Li. Solid and dash lines represent discharging and charging process and cycle numbers are distinguished by colors. The first, second, and 20th cycles are shown as black, red, and blue colors, respectively.

than that of $TiO_2$−B (357 mA h/g) and anatase (245 mA h/g) anodes. But the charging capacity of HCOOH-intercalated titanate is extremely low at merely 10 mA h/g, whereas that of $TiO_2$−B and anatase anodes at the first cycle are 201 and 155 mA h/g, respectively. In addition to different capability of Li ion intercalation, the three electrodes show specific charging/discharging features. The discharging curve of the electrode made from nanosheets heated at 550 °C (top figure in Figure 7) looks like that of a typical discharging curve of anatase electrode with a plateau at 1.78 V versus Li/$Li^+$ and two sloping regions where capacity increases with the decrease of voltage.[22] Thus, we investigated the discharging curve of this electrode at the first cycle comprehensively in these three regions.

When comparing the capacity in the three regions, it was found that the storage capacity in the 1.78−1.00 V region (160 mA h/g, $Li_{0.48}TiO_2$) is much larger than that in the plateau (47 mA h/g, $Li_{0.14}TiO_2$) and the 3.00 to 1.78 V ($Li^+$/Li) region (37 mA h/g, $Li_{0.11}TiO_2$), consistent with a well-known discharging behavior of nanomaterials. There are two signatures in the discharging curve of the electrodes with nanostructure due to high surface/volume ratio: (1) shorter plateau region[8] and (2) gentler slope in the two sloped regions.[22] The steadily decreasing potential before the plateau region is ascribed to the insertion of Li ions into the crystal lattice of anatase $TiO_2$ to form a Li-poor anatase solid solution, $Li_xTiO_2$, where $x$ is strongly dependent on particle size. Wagemaker and co-workers demonstrated that $x = 0.03$ for 120 nm anatase particles, whereas $x$ extended up to 0.1 and 0.21 for 40 and 7 nm anatase nanoparticles.[23] Both the $x$ value and thickness of the nanosheets ($x = 0.11$, 40 nm), are closely related to nanoparticles of size 40 nm ($x = 0.1$). It appears that Li composition of the solid solution depends on the shortest dimension of the nanosheets. One of the features of nano structured electrodes is the shortening of the plateau region, corresponding to the formation of Li-rich $Li_{0.55}TiO_2$, which was observed. It was found that particles of sizes smaller than 40 nm exist as either a Li-poor solid solution phase or Li-rich $Li_{0.55}TiO_2$, whereas the two phases coexist in a single particle for micron-sized prticles.[23,24] As these nanosheets consists of two relatively long dimensions and one short dimension, it is thought that two phases most likely coexist along the preferred plane of growth. This confers both bulk-phase and nanoparticle properties, two-phase equilibrium and high Li composition, that is, dual property. The third potential region, from 1.78−1.00 V contributed the highest capacity, possibly corresponding to the transformation of Li-poor $Li_{0.11}TiO_2$ to $LiTiO_2$, as discussed for nanoparticles.[23]

In previous report, intercalation of Li ions in the 1.78−1.00 V region usually results in stable and reversible capacity on cycling.[22] However, a constant decay of capacity was observed in the 1.78−1.00 V region, from 160 to 85 mA h/g over 20 cycles. Similar phenomena were observed in the $TiO_2$−B electrode. Despite the fact that the discharging capacity of $TiO_2$−B mesoporous nanosheets at the first cycle is highest among the reported $TiO_2$−B to date, the irreversible capacity of initial cycles is large at about 150 and 85 mA h/g at the two initial cycles. We propose that the unusual loss of the reversible capacity is most likely due to three reasons: (1) formation a of solid electrolyte interface layer (SEI), (2) closed interior voids in the nanosheets, and (3) poor electronic contact between Cu foil and $TiO_2$ film due to laminar shape. The SEI formation is usually one of the main factors responsible for irreversible capacity of the anode. However, it seldom occurs on $TiO_2$ electrodes when the low cutoff voltage is greater than 1 V, which is usually considered one of the advantages compared to graphite electrodes.[25] The cycling voltage used in our work is 3−1 V, which can greatly minimize the formation of SEI layer. On the other hand, Hu et al. and Mabuchi et al. have

(22) Jiang, C.; Wei, M.; Qi, Z.; Kudo, T.; Honma, I.; Zhou, H. *J. Power Sources* **2007**, *166*, 239.

(23) (a) Wagemaker, M.; Borghols, W. J. H.; Mulder, F. M. *J. Am. Chem. Soc.* **2007**, *129*, 4323. (b) Wagemaker, M.; Borghols, W. J. H.; van Eck, E. R. H.; Kentgens, A. P. M.; Kearley, G. J.; Mulder, F. M. *Chem.—Eur. J.* **2007**, *13*, 2023.

(24) Wagemaker, M.; Kentgens, A. P. M.; Mulder, F. M. *Nature* **2002**, *418*, 397.

demonstrated that porous carbons such as hierarchically porous carbon and mesocarbon microbeads (MCMB) with many voids demonstrate 3−4 times better intercalation capacity than the theoretical capacity (372 mA h/g) in the initial cycle.[26,27] Nevertheless, the obvious shortcoming is the increase of irreversible capacity because Li ions were trapped in the voids.[27] The $TiO_2$ porous nanosheets electrode acts similarly to porous carbon electrodes. In addition, poor contact between Cu foil and $TiO_2$ film is the most likely factors responsible for irreversible capacity because of the unusually flat shape.

The extremely large irreversible capacity of the anode made from HCOOH-intercalated titanate results from the formation of chemical bonding solid electrolyte interface (CB-SEI) which usually occurs in electrodes between Li ions and surface functional groups. Zheng et al. reported that Li ions will bind to hydrogen-terminated edges of hexagonal carbon fragments like the organolithium molecule $C_2H_2Li_3$, which changes from $sp^2$ to $sp^3$ bonding.[28] But even then, the details of the large irreversible capacity of HCOOH-intercalated titanate is still unknown because of its mysterious structure.

(25) (a) Armstrong, R. A.; Armstrong, G.; Canales, J.; Bruce, P. G. *J. Power Sources* **2005**, *146*, 501. (b) Prosini, P. P.; Mancini, R.; Petrucci, L.; Contini, V.; Villano, P. *Solid State Ionics* **2001**, *144*, 185.
(26) Hu, Y. S.; Adelhelm, P.; Smarsly, B. M.; Hore, S.; Antonietti, M.; Maier, J. *Adv. Funct. Mater.* **2007**, *17*, 1873.
(27) Mabuchi, A.; Tokumits, K.; Fujimoto, H.; Kasuh, T. *J. Electrochem. Soc.* **1995**, *142*, 1041.
(28) Zheng, T.; McKinnon, W. R.; Dahn, J. R. *J. Electrochem. Soc.* **1996**, *143*, 2137.

## Conclusion

$TiO_2$−B and anatase nanosheets were obtained from heat treatment of HCOOH-intercalated titanate, which were synthesized by a simple sol−gel process using TTIP and formic acid as precursors at different temperatures. This is the first time that $TiO_2$−B has been synthesized by such a simple method under mild conditions. Furthermore, the performance of Li-ion intercalation using the three materials as anodes is very good in the initial cycles, even though the irreversible capacity and retention are not as good as that previously reported. This is probably due to the trapping of Li ions in closed interior voids, poor contact,and formation of CB-SEI of Li ion with $TiO_2$ and HCOOH-intercalated titanate electrodes. We believe that this can be overcome to improve the performance of Li-ion batteries by opening the closed interior voids and adjusting preparation of cell anodes. More openly porous nanosheets were occasionally observed in our samples (see the Supporting Information, b and c in Figure S1) and measurements of their Li ion intercalation capacity are in progress.

**Acknowledgment.** The authors thank the National Science Council, ROC Taiwan, and Synchrotron Radiation Research Center, Taiwan, for financially supporting this research under Contract 96-2113-M-007-021-MY3. The authors also thank Jacqueline Kao and Raphael Horvath for English language editing.

**Supporting Information Available:** Additional SEM images (PDF). This material is available free of charge via the Internet at http://pubs.acs.org.

CM802327Z